AAPT PHYSICS EDUCATION | AMERICAN JOURNAL of PHYSICS

Experimental determination of heat capacities and their correlation with theoretical predictions

Waqas Mahmood, Muhammad Sabieh Anwar, and Wasif Zia

Citation: Am. J. Phys. **79**, 1099 (2011); doi: 10.1119/1.3625869
View online: http://dx.doi.org/10.1119/1.3625869
View Table of Contents: http://ajp.aapt.org/resource/1/AJPIAS/v79/i11
Published by the American Association of Physics Teachers

Experimental determination of heat capacities and their correlation with theoretical predictions

Waqas Mahmood, Muhammad Sabieh Anwar,[a] and Wasif Zia
School of Science and Engineering, Lahore University of Management Sciences (LUMS), Opposite Sector U, D. H. A., Lahore 54792, Pakistan

(Received 25 January 2011; accepted 23 July 2011)

We discuss an experiment for determining the heat capacities of various solids based on a calorimetric approach where the solid vaporizes a measurable mass of liquid nitrogen. We demonstrate our technique for copper and aluminum, and compare our data with Einstein's model of independent harmonic oscillators and the more accurate Debye model. We also illustrate an interesting material property, the Verwey transition in magnetite.
[DOI: 10.1119/1.3625869]

I. THEORETICAL MOTIVATION

The departure of the heat capacity from the classical Dulong–Petit law at low temperatures is an example of the success of quantum mechanics.[1] An experiment that is accessible to undergraduates for measuring low temperature heat capacities and correlating results with Einstein's and Debye's, is therefore of pedagogical value. We first summarize the underlying theory.

II. THEORY

A. Einstein model

The nature on the heat capacity of solids can be found in standard texts.[1] In summary, Dulong and Petit showed that the molar heat capacity of metals has the constant value $3R$, where R is the molar gas constant. However, it was found that the heat capacity deviates significantly from this value for low temperatures (below room temperature), especially for elements with mass number greater than 40. This deviation led Einstein to do the first quantum mechanical calculation of the heat capacity.[2,3] He modeled a solid as N independent, three-dimensional oscillators, all with the same fundamental frequency ν, and obtained the temperature dependence of the molar heat capacity C_V as

$$C_V = 3Nk_B\left(\frac{\theta_E}{T}\right)^2 \frac{e^{\theta_E/T}}{\left(e^{\theta_E/T}-1\right)^2}, \tag{1}$$

where k_B is the Boltzmann's constant and $\theta_E = h\nu/k_B$, the Einstein temperature. For high temperatures, $T \gg \theta_E$, C_V approaches $3Nk_B = 3R$ as predicted by the Dulong-Petit law.

B. Debye model

Debye considered the solid as a continuous medium comprising oscillators whose phonon spectrum or density of states $g(\nu)$ obeys the more realistic form, $4\pi\nu^2/c^3$, where c is the propagation speed of a wave in the solid.[4] (In the Einstein model $g(\nu) = \delta\ (\nu - \nu_E)$, where δ is the Dirac's delta function.) Because the speeds vary for the longitudinal (c_l) and the doubly-degenerate transverse (c_t) waves, we write

$$g(\nu)d\nu = 4\pi\nu^2\left(\frac{1}{c_l^3}+\frac{2}{c_t^3}\right)d\nu. \tag{2}$$

If we use Eq. (2) and Planck's formula for the average vibrational energy of the oscillator with frequency ν, the total vibrational energy of the crystal is

$$E = \frac{4\pi k_B^4}{h^3}\left(\frac{1}{c_l^3}+\frac{2}{c_t^3}\right)T^4\int_0^{h\nu_D/k_BT}\frac{x^3}{e^x-1}dx. \tag{3}$$

Here, we have made the substitution $x = h\nu/k_BT$. The Debye frequency ν_D restricts the total number of modes to $3N$. This restriction is achieved by requiring that

$$\int_0^{\nu_D} g(\nu)d\nu = 3N. \tag{4}$$

The cutoff procedure yields

$$\nu_D^3 = \frac{9N}{4\pi}\left(\frac{1}{c_l^3}+\frac{2}{c_t^3}\right)^{-1}. \tag{5}$$

It is useful to define the Debye temperature $\theta_D = h\nu_D/k_B$. The upper limit in the integral in Eq. (3) becomes θ_D/T. Differentiating Eq. (3) with respect to temperature yields

$$C_V = \frac{4\pi k_B^4}{h^3}\left(\frac{1}{c_l^3}+\frac{2}{c_t^3}\right)\frac{\partial}{\partial T}\left(T^4\int_0^{\theta_D/T}\frac{x^3}{e^x-1}dx\right). \tag{6}$$

The heat capacity from the Einstein model is straightforward to calculate, while a numerical integrator is required for Eq. (6).

III. THE EXPERIMENT

We now discuss an experiment for determining C_V for temperatures down to ~100 K. Thompson and White have presented details of a beautiful experiment measuring the latent heat of vaporization of liquid nitrogen and the heat capacity of various metals.[5–7] Their method is based on calorimetric heat exchange between the solid and liquid nitrogen. Our experiment is a straightforward extension of their work. Our added feature is the determination of low temperature heat capacities and a statistical minimization of uncertainties. We show results from experiments performed on Cu

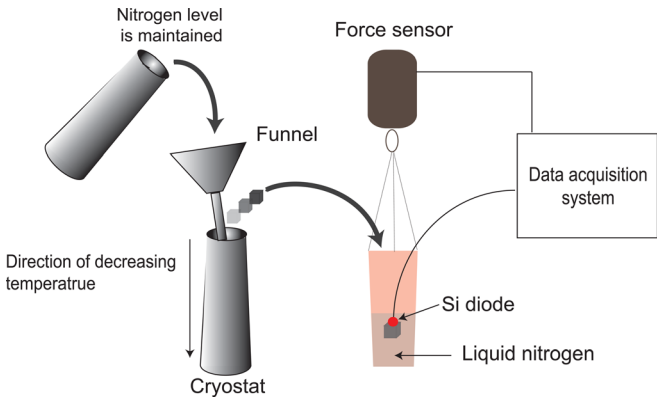

Fig. 1. (Color online) The experimental arrangement. The solid is allowed to thermally equilibrate with the cold nitrogen vapor inside a cryostat and is then swiftly dropped into a container holding liquid nitrogen. The weight of the cup is constantly monitored while the temperature is measured by passing a fixed current through a Si diode and determining the voltage drop across it.

and Al and then illustrate the anomaly in the heat capacity in a ferrimagnetic material at the Verwey transition.

The arrangement of the apparatus is shown in Fig. 1. A force sensor with an accuracy of 0.01 N (1 g) (Vernier Instruments DFS-BTA) is interfaced to the computer and measures the weight of a styrofoam cup containing the continuously vaporizing nitrogen. The solid whose heat capacity is to be determined makes contact with cold nitrogen vapor from the boiling liquid nitrogen placed inside a vacuum flask which serves as the vapor cryostat. The temperature of the solid is monitored by a silicon diode that is secured with teflon tape while thermal grease ensures uniform thermal contact between the sensor and solid. The level of the liquid nitrogen is kept constant by continuous refilling through a funnel. When the desired initial temperature of the solid, T_1, is achieved, it is swiftly dropped into the styrofoam cup containing liquid nitrogen. A rapid hissing sound and effervescence ensues, partly due to the Leidenfrost effect[8] and the

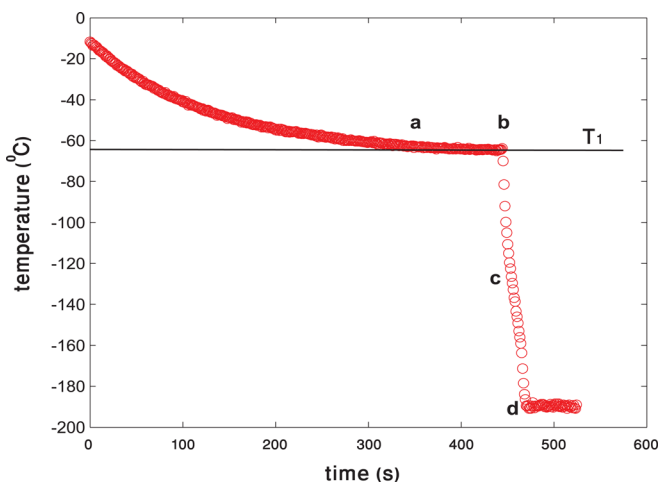

Fig. 2. (Color online) Temperature profile of the solid during the experiment. (a) Represents the point at which the solid achieves the desired temperature inside the vapor cryostat; (b) is the instant when the solid is lifted from the cryostat; (c) is in the region of the decreasing temperature during the solid's transit from the cryostat and subsequent immersion into the cup; and (d) is the point at which the solid equilibrates at 77 K.

cup jostles. Eventually the rapid movement ceases, and the background rate of vaporization is re-established. In equilibrium, the temperature of the solid is 77 K. A representative change of the temperature of the solid during the experiment is illustrated in Fig. 2.

We use an ordinary silicon diode as the cryogenic temperature sensor.[9,10] The underlying principle of the temperature measurement is the diode equation

$$I_f = I_0(T, E_g)[\exp(eV_f/k_BT) - 1], \tag{7}$$

where I_f is the forward-biased current through the diode, V_f is the forward-biased voltage, and I_0 is the reverse saturation current, which depends on temperature and the band-gap E_g. It can be shown[11] that the equation relating the temperature to the diode voltage is given by

$$V_f(T) = \frac{E_g}{2q} - \left[\log \alpha + \frac{3}{2}\log T - \log I_f\right]\frac{k_BT}{q}, \tag{8}$$

with

$$\alpha = \frac{1}{4}\left(\frac{2mk_B}{\pi\hbar^2}\right)^{3/2}\frac{Ak_B}{\tau E_g}, \tag{9}$$

where q, m, A, and τ are, respectively, the charge and mass of the electron, the cross-sectional area of the diode junction, and the momentum scattering time.[1] A plot of V_f versus T is approximately linear from ~100 K to room temperature.

To provide a constant forward biased current $I_f = 10\ \mu$A, a current source can be easily built using an operational amplifier (TL081), Zener diode (2.7 V), and resistors. The circuit is shown in Fig. 3. The resulting voltage V_f is directly read into the computer fitted with a data acquisition card (National Instruments PCI-6221). A LABVIEW program automates the data acquisition.

Note that unlike a wire thermocouple, the diode gives a more stable and accurate measurement for the sample held in the nitrogen vapor. The thermocouple operation is based on the Seebeck effect, wherein a temperature gradient along the length of a conductor results in an emf. The thermocouple wire protruding above the liquid nitrogen surface in the cryostat is placed inside a spatially extended temperature gradient. Therefore, the induced Seebeck voltage originates from the entire thermocouple wire and not only the welded tip making contact with the solid surface. Hence, thermocouple measurements do not represent the temperature of the solid.

An additional concern that might arise is whether the surface temperature truly represents the bulk temperature.

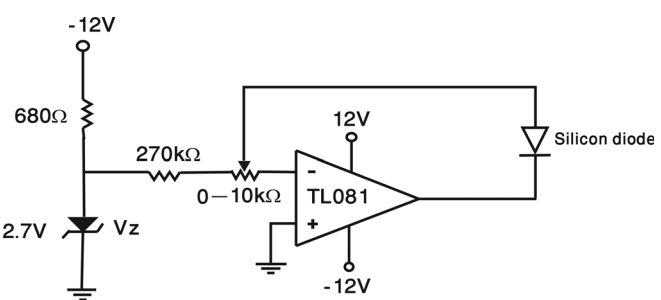

Fig. 3. A hand-built circuit for the current source to provide 10 μA current through the silicon diode. The current is adjusted by the setting of the variable resistor.

Typically our solids are cylinders of diameter 12 mm and length 32 mm. The Si diode measures the surface temperature of the solid, but we can make an intelligent guess about the internal temperature based on the Biot number,[12] HL_c/κ, where H is the coefficient of heat transfer in the presence of nitrogen vapor, L_c is the ratio of the solid volume to its surface area, and κ is the thermal conductivity. The value of H depends on the temperature of the nitrogen near its boiling point,[13] but for a difference greater than 40 K, it is approximately 3000 W/(m^2 K). The dimensionless Biot number is the ratio of the heat exchange between the solid and the surrounding fluid to the heat conduction inside the sample. A ratio smaller than one indicates small resistance to heat conduction inside the sample, enabling the interior of the solid to quickly equilibrate to a uniform temperature. A simple calculation for the Al and Cu samples shows that the Biot number is approximately 0.03 and 0.016, respectively, indicating that the temperature is uniformly distributed within the solid.

Data from a representative experiment are shown in Fig. 4. We construct linear fits to the background evaporation rates before and after immersing the solid. The vertical displacement between these lines is a measure of the additional nitrogen vaporized by the heat transfer from the hotter solid, Δm. The heat capacity is determined from the change in mass:

$$C_V(T_1) = \frac{L_v \Delta m}{n_{\text{moles}}(T_1 - 77)}, \tag{10}$$

where n_{moles} is the number of moles of the solid and L_v is the latent heat of vaporization of nitrogen. To determine the temperature dependence of C_V, we repeat the experiment for different values of T_1 and calculate the corresponding change in Δm.

Figure 5 shows the experimental results for solid copper with $T_1 = 200$ K [Figs. 5(a) and (b)] and $T_1 = 120$ K [see Figs. 5(c) and 5(d)]. The vertical lines are the error bars, u_m, arising from the smallest division on the balance scale, $u_m = 1$ g. We require $\Delta m > u_m$ for our results to be meaningful. In Fig. 5(a) this condition is easily satisfied. The lines before and after immersion do not statistically overlap when extrapolated. The situation changes when T_1 decreases, which result in smaller values of Δm. This trend is illustrated in Fig. 5(c), where the instrumental uncertainties are greater than the change in mass, making it impossible to obtain a reliable value of Δm.

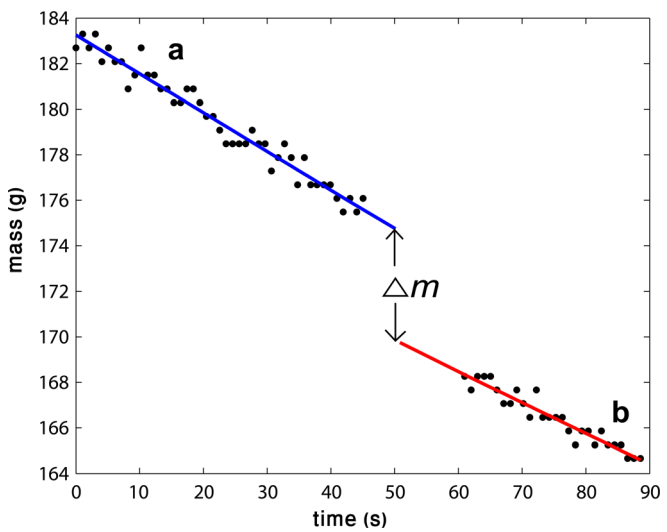

Fig. 4. (Color online) Mass of the vaporizing nitrogen versus time. The set of data points labeled **a** are due to the background evaporation of boiling liquid nitrogen before immersing the solid; the other set of points labeled **b** are due to evaporation after the solid is immersed. The mass of the solid has been subtracted from the second set of plotted points.

To obtain the best results we can use the entire line of data points before and after the immersion of the solid for the determination of Δm, and not just the terminal values at the juncture of the transferral of the solid. Therefore, we are interested in the uncertainties in the slope u_s and the intercept u_i of the lines. These uncertainties can be calculated using[14]

$$u_s^2 \approx \frac{1}{D}\frac{\sum d_i^2}{n-2}, \tag{11}$$

$$u_i^2 \approx \left(\frac{1}{n} + \frac{\bar{m}^2}{D}\right)\frac{\sum d_i^2}{n-2}, \tag{12}$$

where d_i is the deviation of the ith experimental point from the corresponding point on the best-fit line, $\bar{m}$ is the average mass, D is the sum of the squares of the deviations, and n is the total number of points in each line. Computer-based acquisition generates large amounts of data, increasing n and hence reduces the uncertainties in the measurement. Based on u_s and u_i, we can draw confidence bands, with larger n resulting in tighter bands. These bands are illustrated in Figs. 5(b) and 5(d) by a trio of lines; the middle line is the best fit line, and the top and bottom lines represent the extreme.

The best estimate for the reduction in mass is Δm and its uncertainty $u_{\Delta m}$ is based on the maximum (Δm_1) and minimum (Δm_2) differences. These maxima and minima are defined through the inset of Fig. 5(e), $\Delta m_1 = a - f$ and $\Delta m_2 = c - d$. The uncertainty is

$$u_{\Delta m}^2 = (\Delta m_1 - \Delta m)^2 + (\Delta m - \Delta m_2)^2. \tag{13}$$

Our data analysis ensures that $u_{\Delta m} < \Delta m$ even in cases where $u_m > \Delta m$. For example, for $T_1 = 120$ K, the individual mass uncertainty $u_m = 1$ g is larger than the change in mass $\Delta m = 0.72$ g, and the uncertainty calculated after the statistical averaging procedure is $u_{\Delta m} = 0.43$ g, which is smaller than Δm. The uncertainty in C_V, u_{CV} is inferred from $u_{\Delta m}$ using error propagation[14]

$$u_{C_V} = \frac{L_V u_{\Delta_m}}{n_{\text{moles}}(T_1 - 77)}, \tag{14}$$

showing that smaller valuesof T_1 yield higher uncertainties u_{C_V}. This trend is observable in our results.

IV. RESULTS AND DISCUSSION

A. Fits for Cu and Al

Results for the metals Cu and Al are shown in Fig. 6. The data are fitted to Eq. (1), yielding θ_E equal to 278 and 284 K, respectively, which is in reasonable agreement with the accepted values 248 and 306 K).[15] The heat capacity for Al is smaller than Cu, implying higher Einstein temperatures. Students can understand this difference by recognizing that

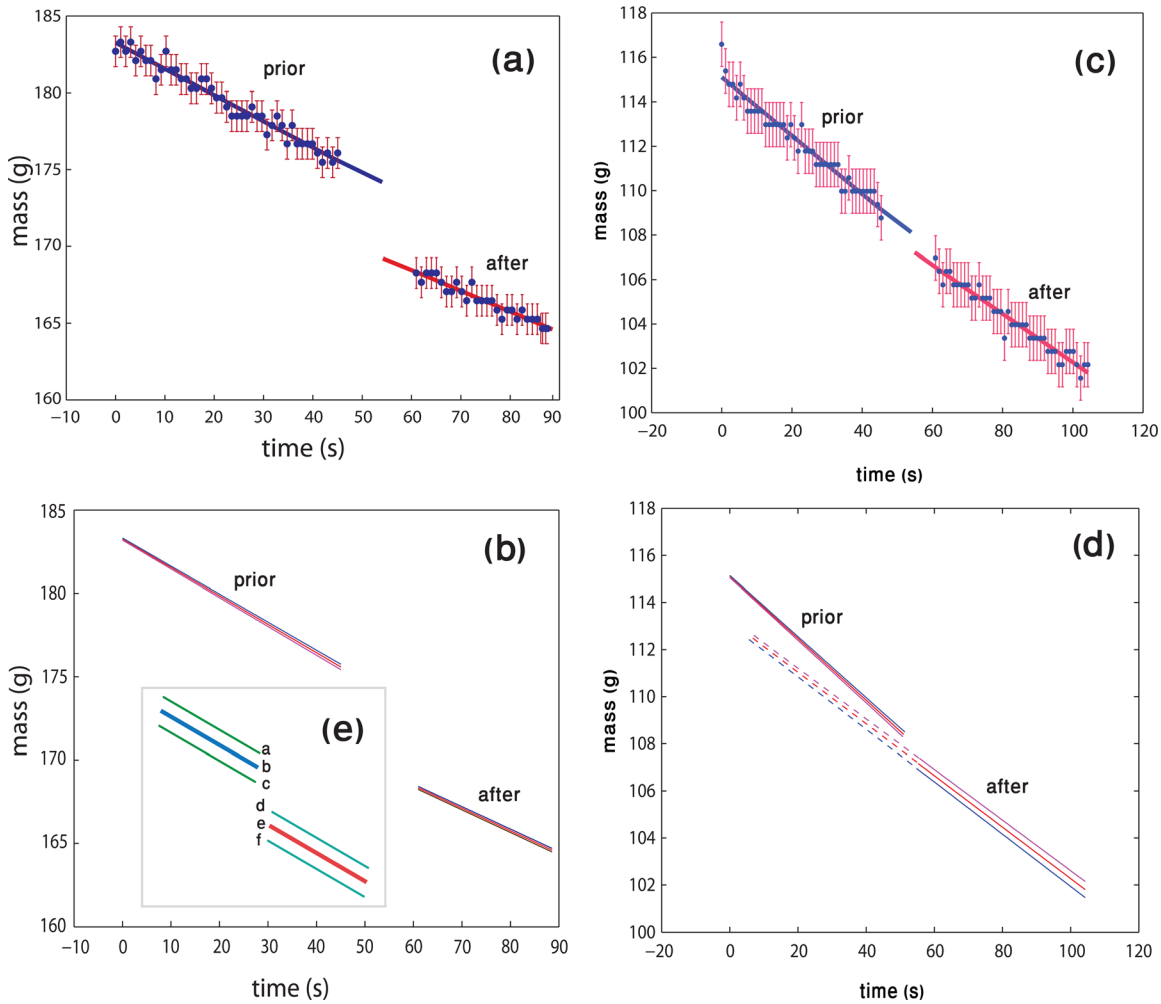

Fig. 5. (Color online) The temporal profile of the evaporating mass for (a) $T_1 = 200$ K and (c) $T_1 = 120$ K. The time-stamped measurements of mass and the uncertainties in each measurement u_m are shown as well as the best linear fits before and after the immersion of the solid sample. For ease of visualization, most of the sample points have been removed. The calculated bands based on the uncertainties in the entire lines are shown in (b) and (d); the individual data points and their uncertainties have been suppressed. For $T_1 = 120$ K, $\Delta m_1 = 5.10$ g, $\Delta m_2 = 4.50$ g, $\Delta m = 4.80$ g, $u_{\Delta m} = 0.45$ g, and $u_{CV} = 0.44$ J/(mol K); for $T_1 = 200$ K $\Delta m_1 = 1.10$ g, $\Delta m_2 = 0.34$ g, $\Delta m = 0.72$ g, $u_{\Delta m} = 0.43$ g, and $u_{C_V} = 1.4\text{J}/(\text{mol K})$.

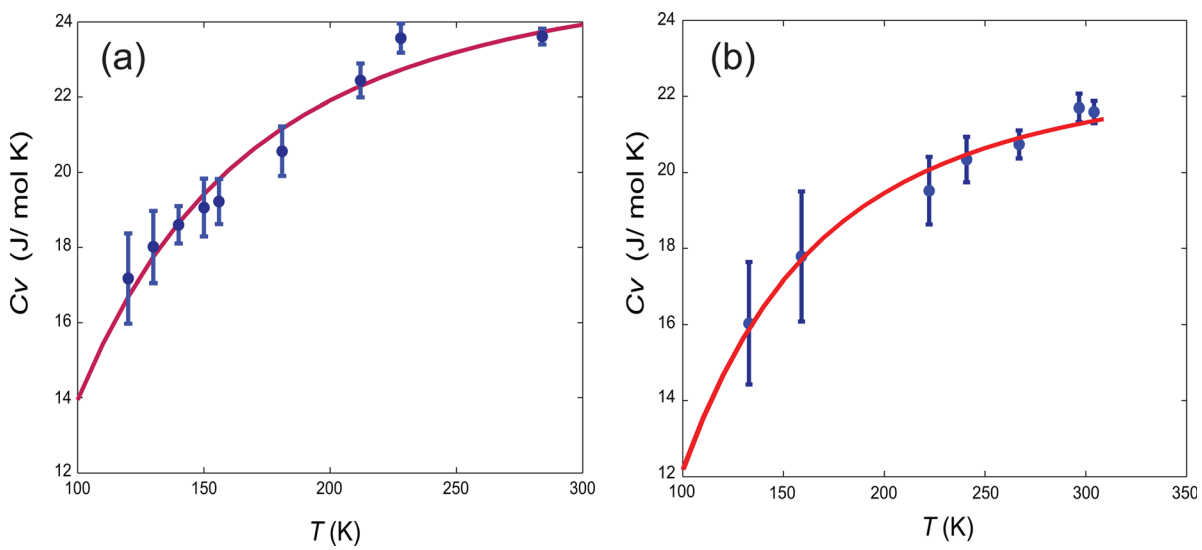

Fig. 6. (Color online) Experimentally determined heat capacities of (a) copper and (b) aluminum and fits to the the Einstein model.

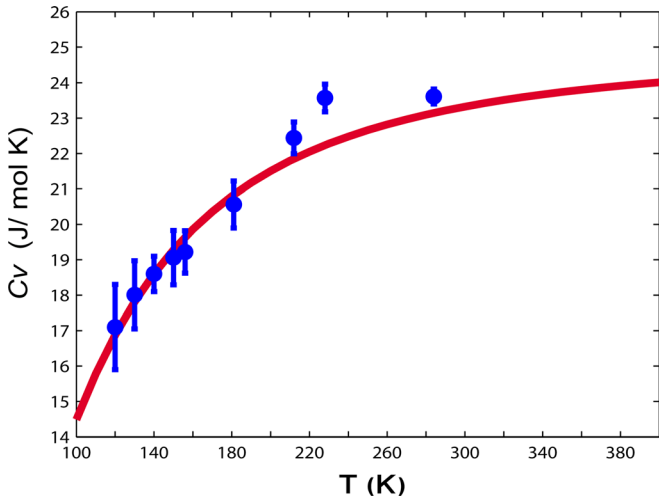

Fig. 7. (Color online) Experimentally determined heat capacities of copper and the best fit to the Debye model.

the Al atom is lighter than Cu (smaller m) and the elastic or effective spring constant k is higher (volume expansivity is lower). Hence the ion frequency $\left(\nu \propto \sqrt{k/m}\right)$ is higher for Al, resulting in a larger value of $\theta_E = h\nu/k_B$.

The experimental data for Cu and the Debye fit with $\theta_D = 350$ K is shown in Fig. 7(a), with the agreement being exceptionally good at lower temperatures. The best estimate of θ_D is found by minimizing the variance between the experimental and numerical values. Our result is in excellent agreement with the published value of 343 K.[1] Results for Al yield $\theta_D = 450$ K, compared to the published value of 428 K.[1]

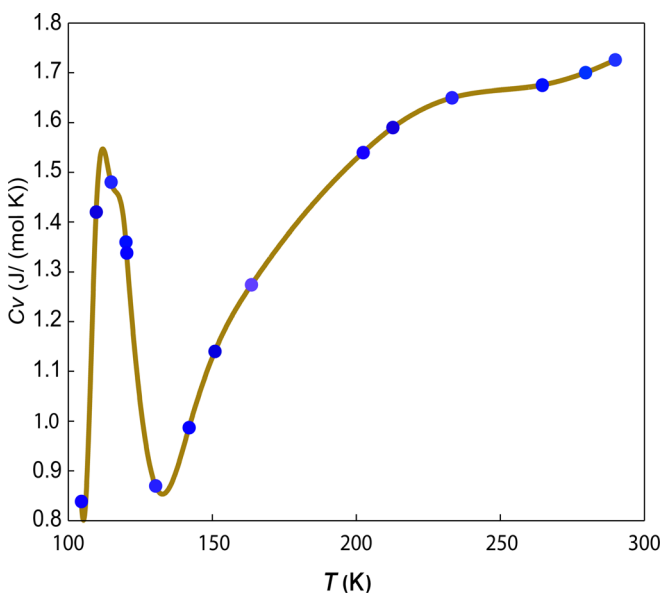

Fig. 8. (Color online) Experimentally determined heat capacities of magnetite, highlighting the change in the heat capacity in the region of the Verwey transition.

For very low temperatures the Debye heat capacity shows a T^3 dependence. The T^3 approximation holds only at temperatures[16] below about $\theta_D/50$, and this dependence is not observed in our experiments which only go to about 100 K. A more expensive helium cryostat would be necessary for observing this behavior.

B. Verwey transition in magnetite

A commonly available ferrite is magnetite, Fe_3O_4, which is well known for its use in ferrite cores of inductors and transformers, and its interesting magnetic, electrical, and structural properties.[17] We highlight an anomaly in the heat capacity of magnetite—the Verwey transition,[18] which occurs at around 120–130 K. At temperatures above the Verwey transition, the ferrite is metallic and electrically conducting, while at lower temperatures it is an electrical insulator, its conductivity less by several orders of magnitude. In addition to the change in electrical conductivity, the heat capacity shows anomalous behavior. Our experimental results are shown in Fig. 8 and agree with Park's original experiment.[19]

[a]Electronic mail: sabieh@lums.edu.pk

[1]C. Kittel, *Introduction to Solid State Physics*, 8th ed. (John Wiley & Sons, New York, 2005).
[2]A. Einstein, "Planck's theory of radiation and the theory of specific heat," Ann. Phys. **22**, 180–190 (1907).
[3]E. Lagendijk, "A simple determination of the Einstein temperature," Am. J. Phys. **68**(10), 961–962 (2000).
[4]P. Debye, "Zur theorie der specifischen wärme," Ann. Phys. **39**, 789–839 (1912).
[5]D. H. Bailey, P. B. Borwein, and S. Plouffe, "On the rapid computation of various polylogarithmic functions," Math. Struct. Comp. Sci. **66**, 903–913 (1997).
[6]R. H. Dittman and M. W. Zemansky, *Heat and Thermodynamics*, 7th ed. (McGraw-Hill, New York, 2007).
[7]C. W. Tompson and H. W. White, "Latent heat and low-temperature heat capacity for the general physics laboratory," Am. J. Phys. **51**(4), 362–364 (1983).
[8]F. L. Curzon, "The Leidenfrost phenomenon," Am. J. Phys. **46**, 825–828 (1978).
[9]P. R. N. Childs, J. R. Greenwood, and C. A. Long, "Review of temperature measurement," Rev. Sci. Instrum. **71**, 2959–2978 (2000).
[10]J. W. Precker and M. A. de Silva, "Experimental estimation of the band gap in silicon and germanium from the temperature voltage curve of diode thermometers," Am. J. Phys. **70**, 1150–1153 (2002).
[11]A. Khalid and M. S. Anwar, "Superconducting quantum interference devices," <physlab.lums.edu.pk>.
[12]F. P. Incropera and D. P. Dewitt, *Fundamentals of Heat and Mass Transfer* (John Wiley & Sons, New York, 2001).
[13]T. Jin, J. Hong, H. Zheng, K. Tang, and Z. Gan, "Measurement of boiling heat transfer coefficient in liquid nitrogen bath by inverse heat conduction method," J. Zhejiang Univ. Sci. A **10**, 691–696 (2009).
[14]G. L. Squires, *Practical Physics* (Cambridge University, New York, 2001).
[15]H. Ledbetter, "Thermal expansion and elastic constants," Int. J. Thermophys. **12**, 637–642 (1991).
[16]Reference 1, p. 124.
[17]B. D. Cullity and C. D. Graham, *Introduction to Magnetic Materials*, 2nd ed. (IEEE Press-Wiley, Piscataway, NJ, 2009).
[18]J. García and G. Subías, "The Verwey transition—a new perspective," Condens. Matter J. Phys. **16**, R145–R178 (2004).
[19]G. S. Parks and K. K. Kelley, "The heat capacities of some metallic oxides," J. Phys. Chem. **30**, 47–55 (1926).